Biophysical Journal, Volume 99

Supporting Material

Chromatin ionic atmosphere analyzed by a mesoscale electrostatic approach

Hin Hark Gan and Tamar Schlick

Supporting Material

Chromatin ionic atmosphere analyzed by a mesoscale electrostatic approach

Hin Hark Gan and Tamar Schlick
Department of Chemistry, New York University

S1. Monte Carlo sampling of chromatin conformations

We use the mesoscale model to sample chromatin conformations in monovalent and divalent salts using a Monte Carlo approach. The chromatin energy terms include Lennard-Jones and electrostatic interactions, as well as bending and torsion terms. The details of the energy terms and associated parameters have been described previously (1). The monovalent salt effect on chromatin interactions is treated via effective salt-dependent charges derived from our DiSCO program (2;3). Briefly, DiSCO uses the Debye-Hückel approximation of the nucleosome's electric field and finds the optimal surface charges to approximate the electric field of the full atom representation of the nucleosome core at distances > 5 Å from the surface sites. The optimization is achieved through the truncated-Newton TNPACK optimization routine (4-6), integrated within the DiSCO package, as described by Beard and Schlick (2) and Zhang et al. (3). The electric field is computed using the nonlinear Poisson-Boltzmann equation solver DelPhi (7-9).

At a given monovalent salt concentration, the effective charges for the sites on the nucleosome core, histone tails, and linker histone are computed using the DiSCO program; the effective charges on DNA beads are modeled using Stigter's estimates (10). The divalent salt effect is treated phenomenologically based on experimental studies on DNA bending (11;12), as describe in our previous studies (13). Specifically, we reduce the repulsion among linker DNA in linker/linker interactions by setting an inverse Debye length of κ=2.5 nm^{-1} to allow DNA to almost touch one another, and reduce the persistence length of the linker DNA sequences from 50 to 30 nm according to experimental findings (11;12).

We employ four different Monte Carlo (MC) moves – pivot, translation, rotation, and tail regrowth – to efficiently sample from the ensemble of oligonucleosome conformations at constant temperature. Global pivot moves are implemented by randomly choosing one of the linker beads or nucleosome cores and rotating from a uniform distribution within [0,20°] about a random axis passing through the chosen component. A similar procedure is applied for local translation and rotation moves. In a translation move, the shift along the axis is a distance sampled from a uniform distribution in the range [0,6 Å]; in a rotation displacement, it is rotated about the axis by an angle uniformly sampled from the range [0,36°]. All three MC moves are accepted/rejected based on the standard Metropolis criterion. We employ the configurational bias MC method (14;15) to efficiently sample histone-tail conformations. Specifically, we randomly select a histone chain and regrow it bead-by-bead by using the Rosenbluth scheme (16), beginning with the bead attached to the nucleosome core. The pivot, translation, rotation, and tail regrowth moves are attempted with frequencies of 0.2:0.1:0.1:0.6, respectively (1;17). Simulations are run on a 2.33 GHz Intel-Xeon machine. Typically, a 10-million step simulation for 12- and 24-core oligonucleosomes takes 3-5 and 4-6 CPU days, respectively. For better statistics, we typically run 12 simulations of this length for each condition.

We have examined MC convergence in two recent works (18;19) from different starting conformations and various conditions, in terms of global and local energetic and geometric quantities. We monitor MC convergence using chromatin energy and various geometric angle parameters. The main conclusion from our MC simulations for 24-core oligonucleosomes is that

the energy converges by 10 to 15 million MC steps and the geometric quantities by 20-40 million steps depending on the DNA linker length and starting zigzag and solenoid structures (19). For 12-core chromatin, convergence of trajectories is faster, occurring typically around 10 millions MC steps.

S2. Internucleosome interaction matrix and intensity

To probe the interactions between nucleosomes, we use internucleosome interaction matrix and intensity. The interaction matrix $I'(i, j)$ is defined as the fraction of configurations that nucleosome pairs i and j interact with one another via all interactions involving the histone tails (17). A tail is considered to be in contact with a chromatin component if the shortest distance between its beads and that of the component is smaller than 80% of the excluded volume size parameter. The one-dimensional internucleosome interaction intensity is defined by the projection $I(k) = \sum_i I'(i, i \pm k)$, which represents the interaction intensity between nucleosomes separated by k linkers. An intensity peak at k = 2 corresponds to an idealized two-start zigzag structure, peaks at k = 1 and 6 indicate a solenoid structure, and peaks at k = 5 and 6 represent an interdigitated solenoid structure (13).

S3. Analysis of charge distribution and fluctuations

We also consider fractional distributions of shielding charges and their fluctuations to help identify the dominant effects of counterions and their variations due to interactions in the chromatin structure. We compute the fraction of shielding charges for each chromatin component as follows:

$$\overline{Q}_\alpha = \sum_j^N Q_{\alpha j} \Big/ \sum_{\alpha,j}^N Q_{\alpha j} \qquad \text{(S1)}$$

where Q_α is net local shielding charge of component α and core position j, and N is the number of cores. For the 12-core chromatin conformation at 5 million MC steps in 0.15M NaCl salt (Fig. 2, upper row), the shielding charge fractions are 0.835, 0.103, 0.029, and 0.033 for nucleosome core, linker DNA, histone tails, and linker histone, respectively. These charge fractions are not sensitive to monovalent salt concentrations in the range of 0.05M to 0.3M investigated (see all values in Table S1). Rather, they are correlated with the values of bare charges on the chromatin components. We also find that the charge fractions are also not sensitive to the two chromatin conformations examined. These results imply that the average shielding charges of chromatin components are predominantly determined by the charges on the macromolecule with minor changes due to conformational fluctuations.

For the same 12-core chromatin conformation at 5 million MC steps in 0.15M divalent salt, the charge fractions are 0.836, 0.105, 0.013, and 0.046 for nucleosome core, linker DNA, histone tails, and linker histone, respectively (see values for different concentrations in Table S2). These values are similar to those for monovalent salt. Thus, the fractional charge distributions show that the dominant role of counterions is to neutralize the nucleosome core and linker DNA; the histone tails and linker histone play secondary roles in enhancing chromatin compaction (20).

The distribution of shielding charges is also influenced by the conformational flexibility of components like the histone tails and linker DNA. For example, compaction of nucleosome cores and the variable conformations of histone tails could indicate fluctuating shielding charges

in the chromatin structure. The average charge distribution $\overline{Q}_\alpha$ is not appropriate for measuring charge fluctuations because it is primarily determined by the bare charges of the components. To measure fluctuations of shielding charges, we define the normalized correlation between shielding charges around chromatin components as follows:

$$\hat{Q}_{\alpha\beta} = \sum_{i=1}^{N} \left(\hat{Q}_{\alpha i} - 1\right)\left(\hat{Q}_{\beta i} - 1\right) \tag{S2}$$

where $\hat{Q}_{\alpha i} = Q_{\alpha i} / \langle Q_\alpha \rangle$ and $\langle Q_\alpha \rangle = \frac{1}{N}\sum_j^N Q_{\alpha j}$. $\hat{Q}_{\alpha\beta}$ is a symmetric measure of the fluctuations of shielding charges for any two chromatin components α and β.

We examine both the diagonal $\hat{Q}_{\alpha\alpha}$ and off-diagonal $\hat{Q}_{\alpha\beta}$ elements. We label the four chromatin components nucleosome core (C), linker DNA (D), histone tails (T), and linker histone (LH) as α=1, 2, 3 and 4, respectively. For both monovalent and divalent salts, we find that the diagonal component $\hat{Q}_{33}$ (T/T) is generally larger than $\hat{Q}_{44}$ (LH/LH), which in turn is larger than $\hat{Q}_{22}$ (D/D), and $\hat{Q}_{11}$ (C/C). For the conformation at 5 million MC steps in 0.15M monovalent salt, the values of $\hat{Q}_{11}$ (C/C), $\hat{Q}_{22}$ (D/D), $\hat{Q}_{33}$ (T/T), and $\hat{Q}_{44}$ (LH/LH) are 0.261, 0.582, 40.50, and 2.235, respectively (see symmetric matrix in Table S3). This implies that shielding charge fluctuations are the largest for the histone tails due to their conformational flexibility, followed by linker histone, linker DNA, and nucleosome core. Since the nucleosome core is rigid, it has the least amount of charge fluctuations, which are generated by core-core interactions. The magnitude of charge fluctuations for linker histones is likely due to their proximity to the linker DNA.

The off-diagonal elements $\hat{Q}_{\alpha\beta}$ express the extent to which shielding charges around two different components are correlated. Thus, they help quantify the higher-order changes in shielding charge patterns as a function of chromatin conformation and salt valence. Element values can be positive or negative depending on the net charge of the counterions. We find the largest off-diagonal element is $\hat{Q}_{13}$ (C/T) and the elements with the smallest magnitudes are $\hat{Q}_{14}$ (C/LH) and $\hat{Q}_{12}$ (C/D); the elements $\hat{Q}_{23}$ (D/T), $\hat{Q}_{24}$ (D/LH), and $\hat{Q}_{34}$ (T/LH) have intermediate values. These relative values indicate that the core-tail shielding charges are more strongly correlated than for core-LH and core-DNA. This is expected because the flexible tails are attached to the parent nucleosome core providing ample opportunities for their ionic atmospheres and therefore shielding charges to interfere (see Fig. 2). In contrast, the linker DNA and linker histones are almost rigidly attached to the core yielding small shielding charge variations. The DNA-tail and tail-LH elements have intermediate correlation strengths because these chromatin components participate in longer range tertiary interactions which can interfere with their ionic atmospheres. In particular, Fig. 2 shows that the H3 tails (blue) interact with linker DNA (gold).

S4. Computation of the energy due to salt effects for 24-core arrays

The accuracy of the energy due to the salt effects is influenced by the grid resolution. Unlike the nucleosome core and 12-core oligonucleosome systems, we use a finer 301×301×301 grid for the

larger 24-core nucleosome arrays. For the monovalent salt case, we calculate all structures with a box fill percentage (DelPhi's perfil parameter) of 30%. We have also computed structures at box fill of 25% and 40%. Comparison of salt energy values shows that a box fill of 30% is adequate. For the mixed salt case, we use lower grid resolutions with box fill values ranging from 8% to 20%; note that for a given structure the salt energy is always calculated at the same grid resolution or box fill value. The use of nonuniform box fill values is necessitated by the lack of converged solutions of the PBE for larger box fill values when performing focusing electrostatic potential computations. This is likely caused by the use of the approximate Coulombic boundary condition and the numerical instability associated with multivalent ions. These convergence issues illustrate that other strategies for solving the PBE need to be considered for large, highly charged systems with multivalent ions.

S5. Justification of model resolutions of chromatin components

As discussed extensively in our previous papers, each component of our mesoscale chromatin model was modeled separately to reasonably reproduce associated geometric, electrostatic, and conformational properties. This model is capable of predicting both global and local aspects such as folding/unfolding behavior under various salt conditions, detailed structural features of the 30nm fiber that have been verified experimentally, interaction patterns of histone tails, and effects due to linker histone.

We represent the nucleosome core structure (21) (without the histone tails) using 300 uniformly-spaced surface beads of radius of 6 Å to approximate the structure's irregular shape (3). The salt-dependent charges of the beads are determined using our DiSCO (Discrete Surface Charge Optimization) software (2) to approximate the nucleosome core's electric field calculated from the Poisson-Boltzmann equation (PBE) using a Debye-Hückel point charge approximation. Nucleosome models with a lower number of surface beads lead to a larger discrepancy with the electric fields of the all-atom nucleosome model (electric field residual $R > 10\%$).

The linker DNA connecting adjacent nucleosome cores is treated using the discrete elastic wormlike chain model (22). Each charged bead segment represents 3-nm (~9 bp) of relaxed DNA. A bead radius of ~15 Å was chosen to match the overall rotational diffusion of DNA (22).

The histone tail bead radius of 9 Å was determined by adjusting the model's force field parameters to mimic the Brownian dynamics (Q. Zhang, PhD Thesis, NYU, 2005) of the protein subunit model (a finer bead model) of Levitt and Washel (23). Namely, starting from the amino-acid/subunit model of Warshel and Levitt (23), for each histone tail (where each residue is a bead), we simulated Brownian dynamics of the tails and further coarse-grained the polymers to obtain parameterized protein beads (charges, excluded volume, harmonic stretching and bending) that reproduced configurational properties of the subunit model. Our chromatin simulation studies have shown that this histone tail model does give rise to stacked nucleosomes in compact chromatin fibers and that the H4 tails mediate the strongest inter-nucleosomal interactions due to their favorable location on the nucleosome core, especially at high salt (17). Our detailed testing studies also showed that the flexible tail model reproduces experimental data better than the former rigid-tail model.

Our linker histone model is essentially designed to mimick the experimental DNA stem formation, as shown in a recent work (13). The simple 3-bead model of linker histone thereby incorporates the strong interactions between linker DNA and linker histone, which could not be modeled in our previous chromatin studies. We have shown that such a linker histone model can

account for further compaction of the chromatin fiber compared with the chromatin model without linker histone, as known experimentally (13). The linker histone model can certainly be improved to incorporate flexibility and variable attachment points on the nucleosome.

Reference List

1. Arya,G., Zhang,Q. and Schlick,T. (2006) Flexible histone tails in a new mesoscopic oligonucleosome model. *Biophys. J.*, **91**, 133-150.

2. Beard,D.A. and Schlick,T. (2001) Modeling salt-mediated electrostatics of macromolecules: The discrete surface charge optimization algorithm and its application to the nucleosome. *Biopolymers*, **58**, 106-115.

3. Zhang,Q., Beard,D.A. and Schlick,T. (2003) Constructing irregular surfaces to enclose macromolecular complexes for mesoscale modeling using the Discrete Surface Charge Optimization (DiSCO) algorithm. *Journal of Computational Chemistry*, **24**, 2063-2074.

4. Schlick,T. and Fogelson,A. (1992) Tnpack - A Truncated Newton Minimization Package for Large-Scale Problems .1. Algorithm and Usage. *Acm Transactions on Mathematical Software*, **18**, 46-70.

5. Schlick,T. and Fogelson,A. (1992) Tnpack - A Truncated Newton Minimization Package for Large-Scale Problems .2. Implementation Examples. *Acm Transactions on Mathematical Software*, **18**, 71-111.

6. Xie,D.X. and Schlick,T. (1999) Efficient implementation of the truncated-Newton algorithm for large-scale chemistry applications. *Siam Journal on Optimization*, **10**, 132-154.

7. Gilson,M.K. and Honig,B. (1988) Calculation of the total electrostatic energy of a macromolecular system: solvation energies, binding energies, and conformational analysis. *Proteins*, **4**, 7-18.

8. Sharp,K.A. and Honig,B. (1990) Electrostatic interactions in macromolecules: theory and applications. *Annu. Rev. Biophys. Biophys. Chem.*, **19**, 301-332.

9. Sharp,K.A. and Honig,B. (1990) Calculating Total Electrostatic Energies with the Nonlinear Poisson-Boltzmann Equation. *Journal of Physical Chemistry*, **94**, 7684-7692.

10. Stigter,D. (1977) Interactions of highly charged colloidal cylinders with applications to double-stranded. *Biopolymers*, **16**, 1435-1448.

11. Baumann,C.G., Smith,S.B., Bloomfield,V.A. and Bustamante,C. (1997) Ionic effects on the elasticity of single DNA molecules. *Proc. Natl. Acad. Sci. U. S. A*, **94**, 6185-6190.

12. Rouzina,I. and Bloomfield,V.A. (1998) DNA bending by small, mobile multivalent cations. *Biophys. J.*, **74**, 3152-3164.

13. Grigoryev,S.A., Arya,G., Correll,S., Woodcock,C.L. and Schlick,T. (2009) Evidence for heteromorphic chromatin fibers from analysis of nucleosome interactions. *Proc. Natl. Acad. Sci. U. S. A*, **106**, 13317-13322.

14. Frenkel,D., Mooij,G.C.A.M. and Smit,B. (1992) Novel Scheme to Study Structural and Thermal-Properties of Continuously Deformable Molecules. *Journal of Physics-Condensed Matter*, **4**, 3053-3076.

15. Depablo,J.J., Laso,M. and Suter,U.W. (1992) Simulation of Polyethylene Above and Below the Melting-Point. *Journal of Chemical Physics*, **96**, 2395-2403.

16. Rosenbluth,M.N. and Rosenbluth,A.W. (1955) Monte Carlo calculations of the average extension of molecular chains. *J. Chem. Phys.*, **23**, 356-359.

17. Arya,G. and Schlick,T. (2006) Role of histone tails in chromatin folding revealed by a mesoscopic oligonucleosome model. *Proc. Natl. Acad. Sci. U. S. A*, **103**, 16236-16241.

18. Schlick,T. and Perisic,O. (2009) Mesoscale simulations of two nucleosoem-repeat length oligonucleosomes. *Phys. Chem. Chem. Phys.*, **11**, 10729-10737.

19. Perisic,O., Collepardo,R. and Schlick,T. (2010) Modeling studies of chromatin fiber structure as a function of DNA linker length. *J. Mol. Biol. (submitted)*.

20. Arya,G. and Schlick,T. (2009) A tale of tails: how histone tails mediate chromatin compaction in different salt and linker histone environments. *J. Phys. Chem. A*, **113**, 4045-4059.

21. Luger,K., Mader,A.W., Richmond,R.K., Sargent,D.F. and Richmond,T.J. (1997) Crystal structure of the nucleosome core particle at 2.8 A resolution. *Nature*, **389**, 251-260.

22. Allison,S.A. (1986) Brownian Dynamics Simulation of Wormlike Chains - Fluorescence Depolarization and Depolarized Light-Scattering. *Macromolecules*, **19**, 118-124.

23. Levitt,M. and Warshel,A. (1975) Computer simulation of protein folding. *Nature*, **253**, 694-698.

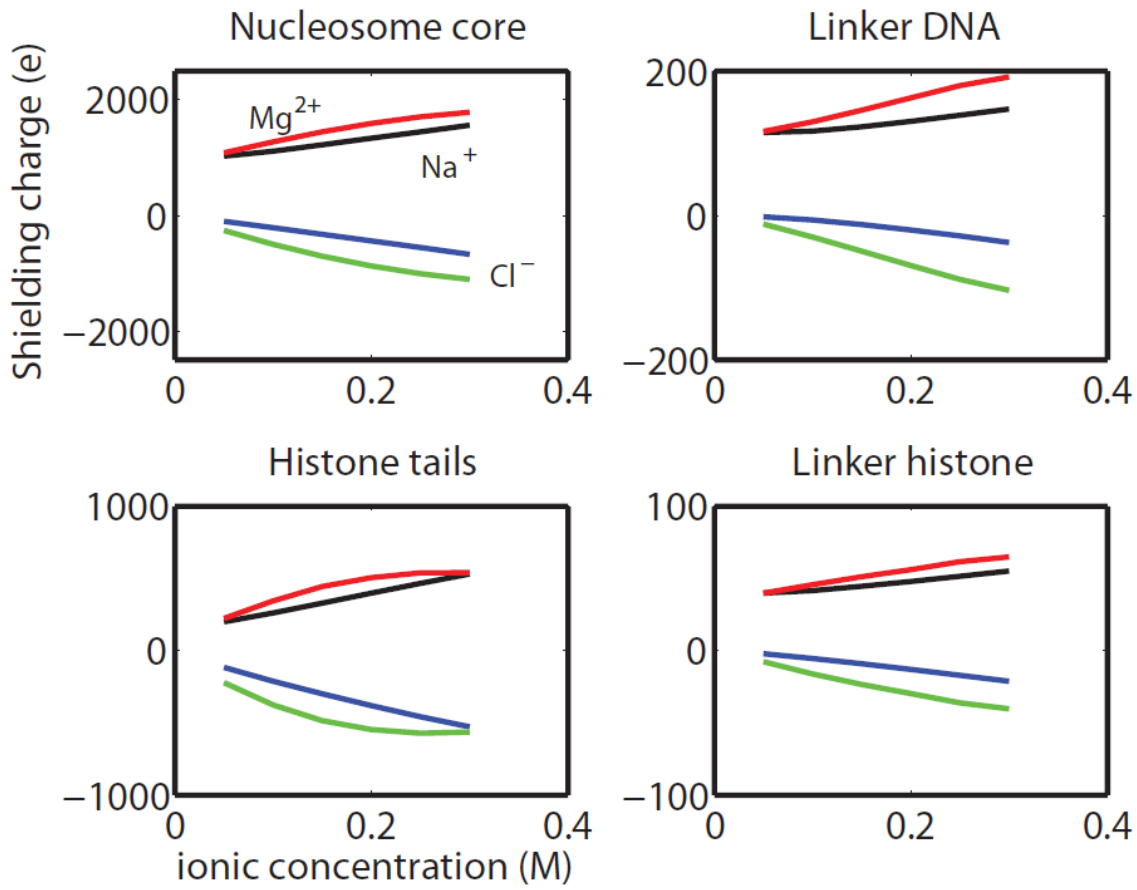

Fig. S1
Comparison of total shielding charges around the four chromatin components of a 12-core chromatin conformation at 5 million Monte Carlo steps sampled at 0.15M NaCl salt (Fig. 2, upper row). The shielding charges are computed for 0.15M NaCl and 0.15M $MgCl_2$ salt conditions. Only shielding charges within a shell of 5 Å beyond the exclusion zone around each interaction site of each chromatin component are counted (see Fig. 1B). The charges for Na^+ and Cl^- of NaCl salt are shown as black and blue lines, respectively, and the charges for Mg^{2+} and Cl^- of $MgCl_2$ salt as red and green lines.

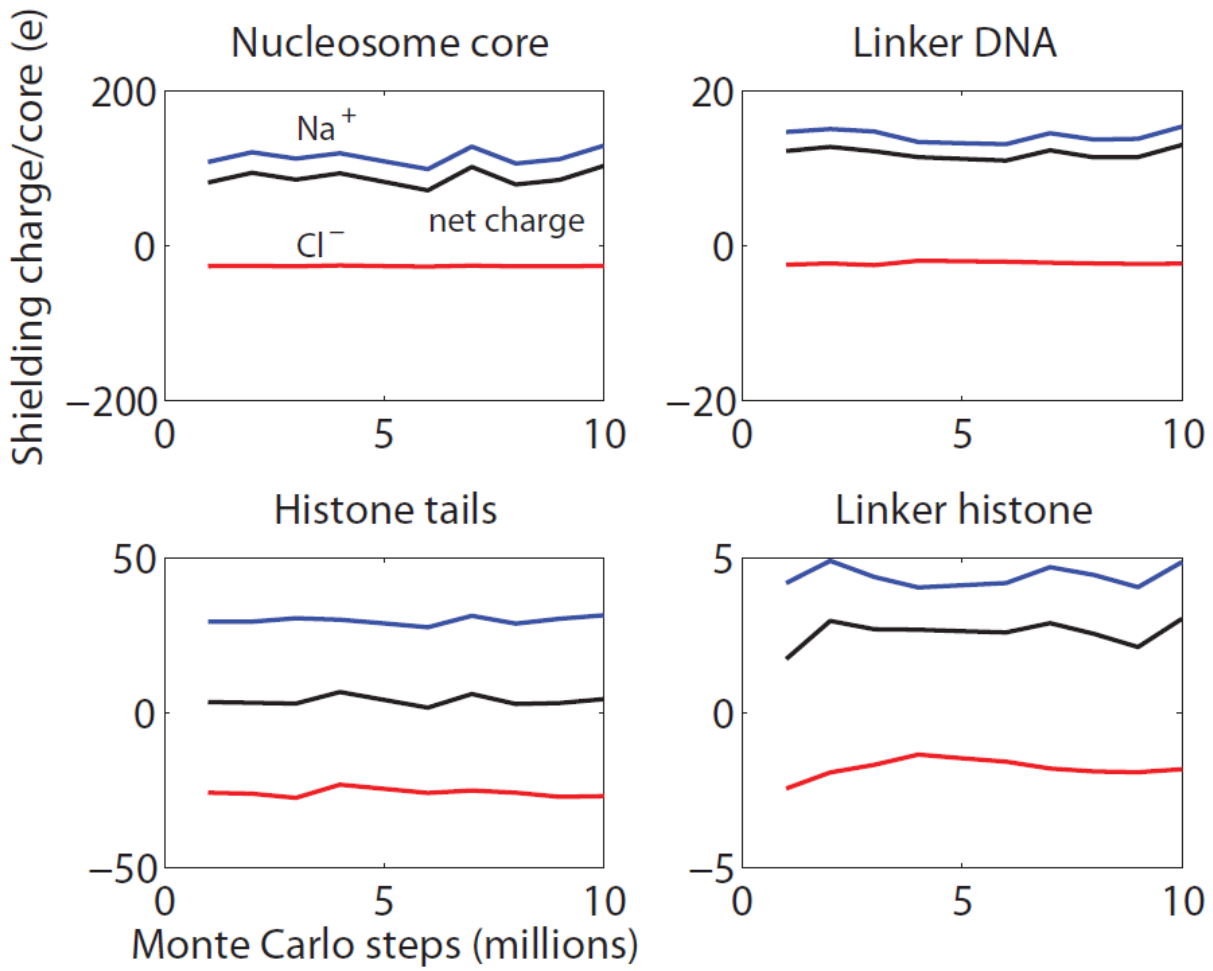

Fig. S2
Shielding charges around the four chromatin components of chromatin structures from the Monte Carlo trajectory with 0.15M NaCl salt (Fig. 4, upper panel). The net or excess (black line), Na^+ (blue) and Cl^- (red) shielding charges are plotted as a function of chromatin core position. Only shielding charges within a shell of 5 Å beyond the exclusion zone around each interaction site of each chromatin component are counted (see Fig. 1B).

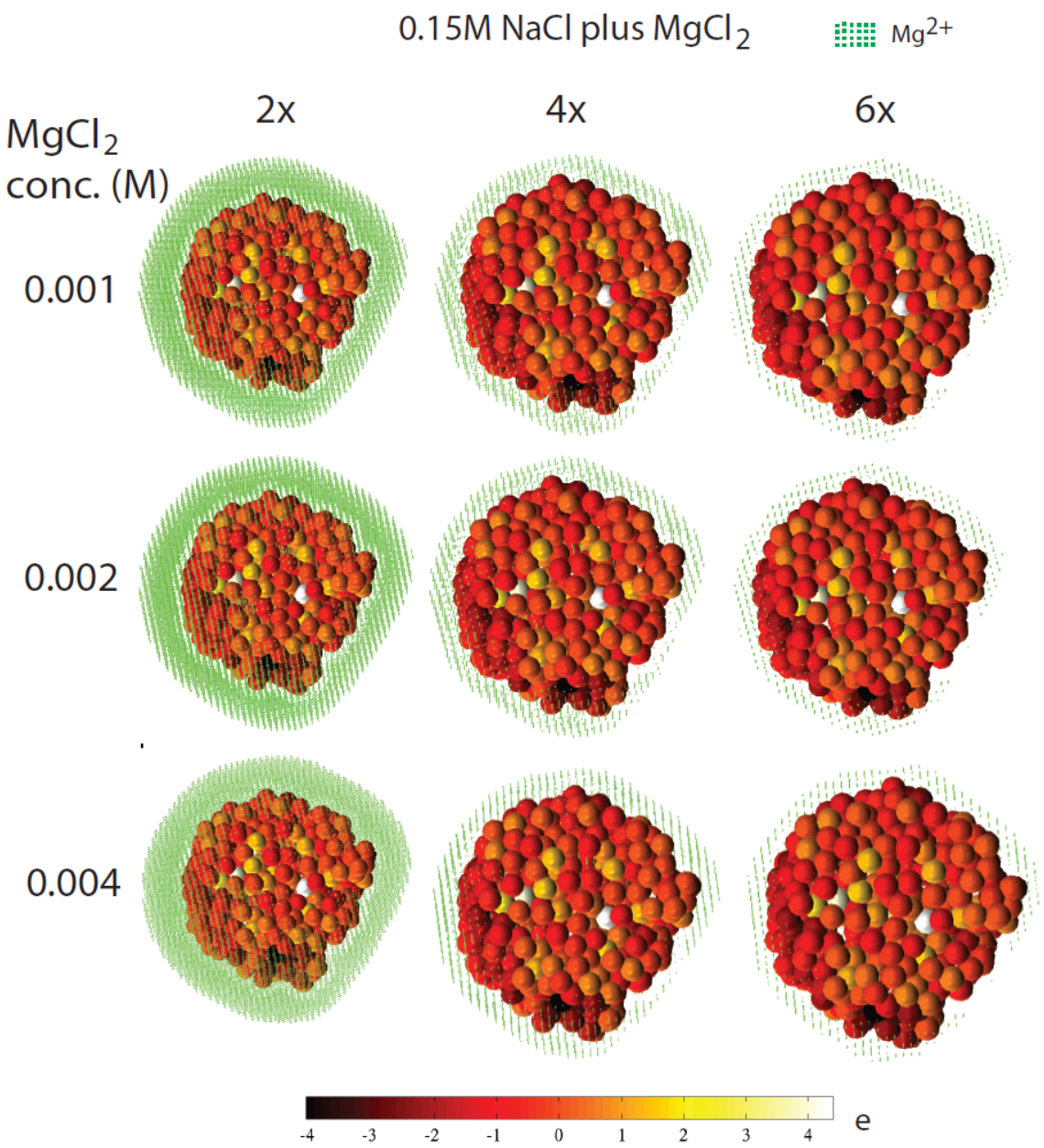

Fig. S3.
Distributions of Mg^{2+} (green dots) in mixed 0.15M NaCl and $MgCl_2$ salts at 2 (first column), 4 (second column) and 6 (third column) times the bulk magnesium concentration. Shown are results for three bulk $MgCl_2$ concentrations: 0.001M (first row), 0.002M (second row) and 0.004M (third row).

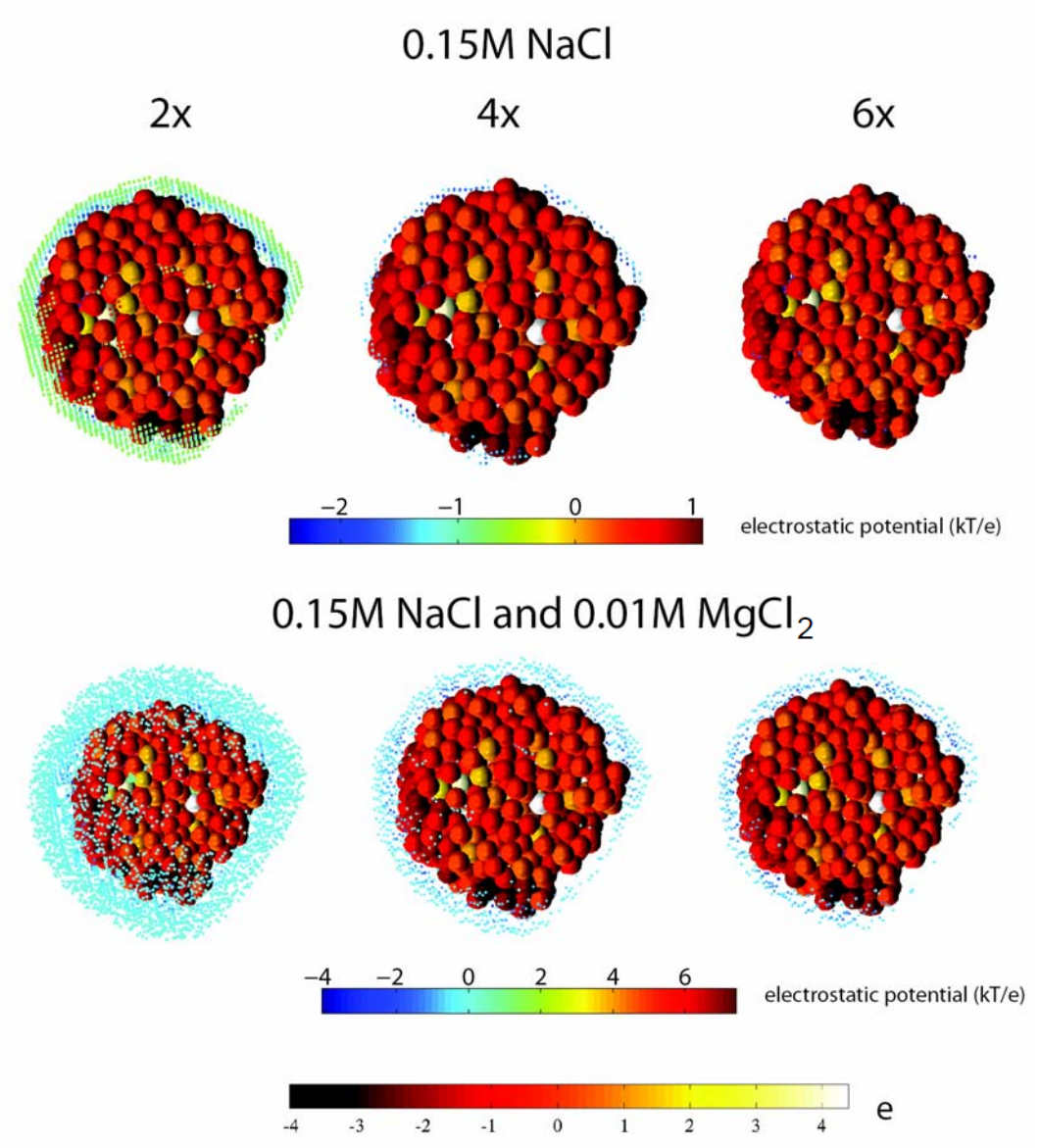

Fig. S4.
Electrostatic potentials near the nucleosome core corresponding to the cutoff ion concentrations of 2, 4 and 6 times the bulk concentration of 0.15M NaCl (upper row) and 0.01M $MgCl_2$ (lower row) in Figure 1. The electrostatic potentials (units of kT/e) and nucleosome bare charges (e) are indicated using different color scales.

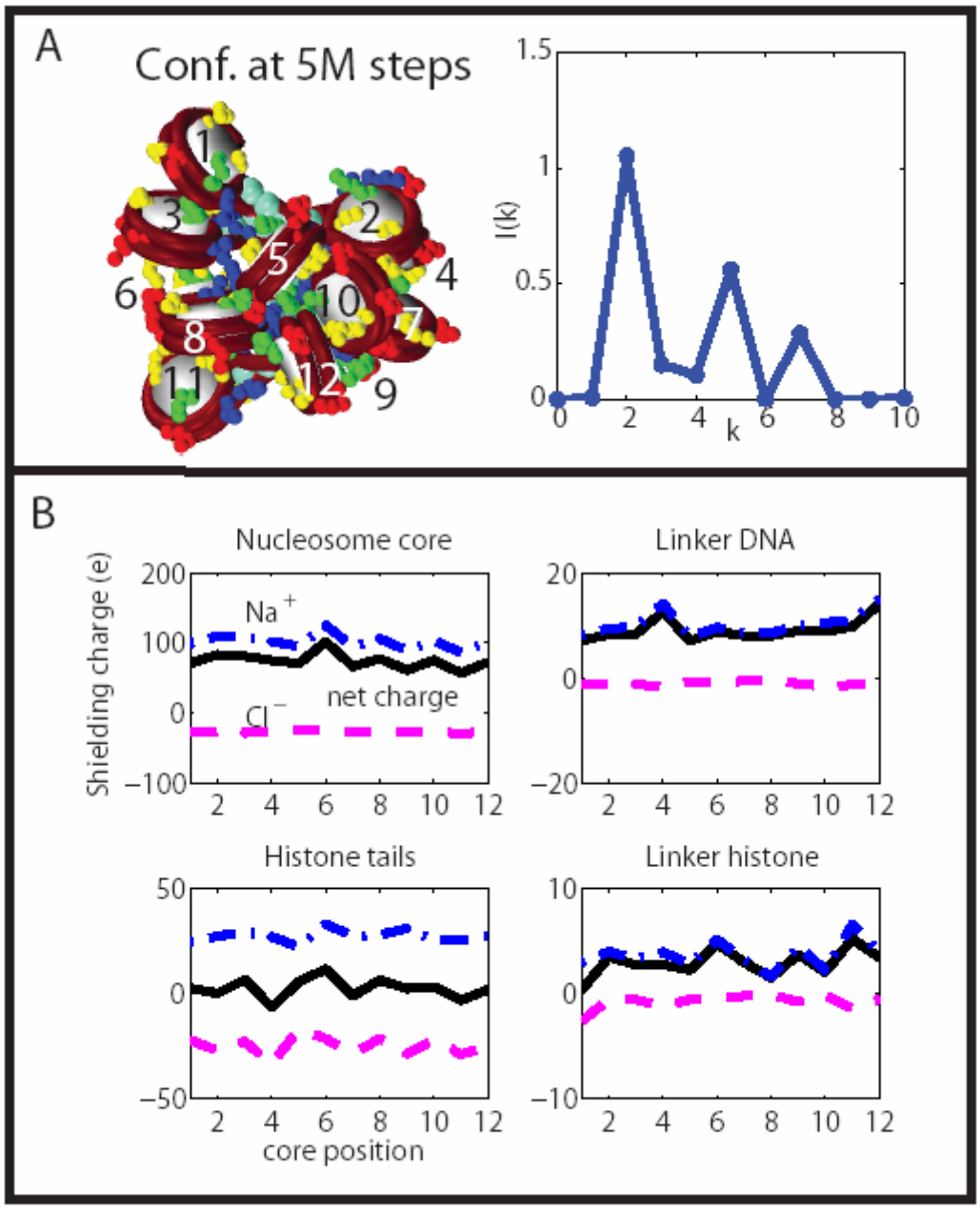

Fig. S5 (Fig. 3 in paper)
A: A 12-core chromatin conformation at 5 million MC steps sampled at 0.15M NaCl salt and its internucleosome interaction intensity I(k) showing a dominant zigzag feature (peak at k = 2).
B: Shielding charges around the four chromatin components of chromatin structure in A. The net (black line), Na^+ (blue dash-dot line) and Cl^- (magenta dash line) shielding charges are plotted versus nucleosome core position.

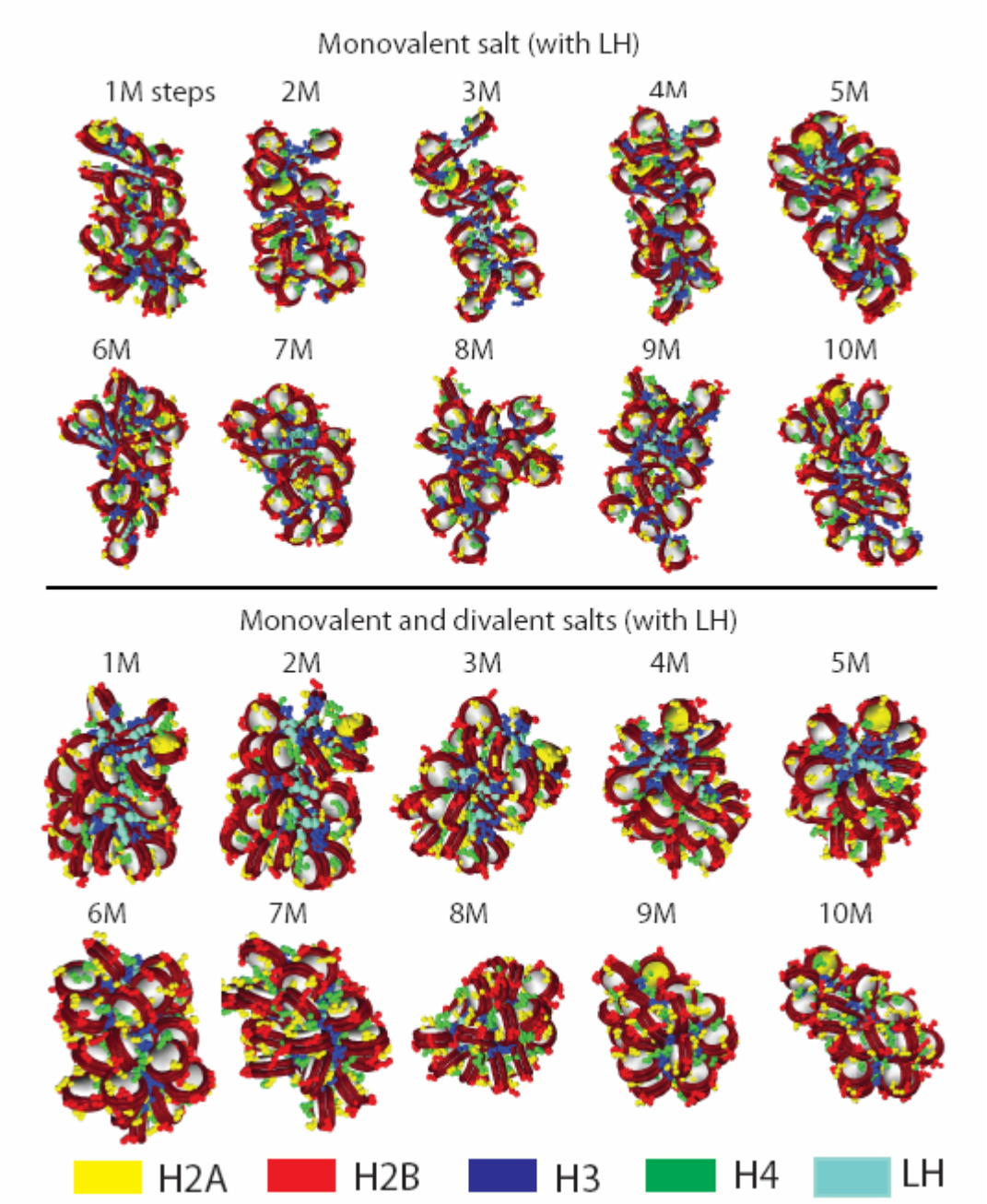

Fig. S6 (Fig. 4 in paper)
Ten snapshots of chromatin structures from two MC simulations of a 24-core nucleosome array at 0.15M NaCl salt condition (upper set of structures) and mixed 0.15M NaCl and $MgCl_2$ salt condition (lower set). The starting configuration is a zigzag structure. The chromatin color scheme is the same as in Fig. 2; the first nucleosome core, where visible, is colored yellow.

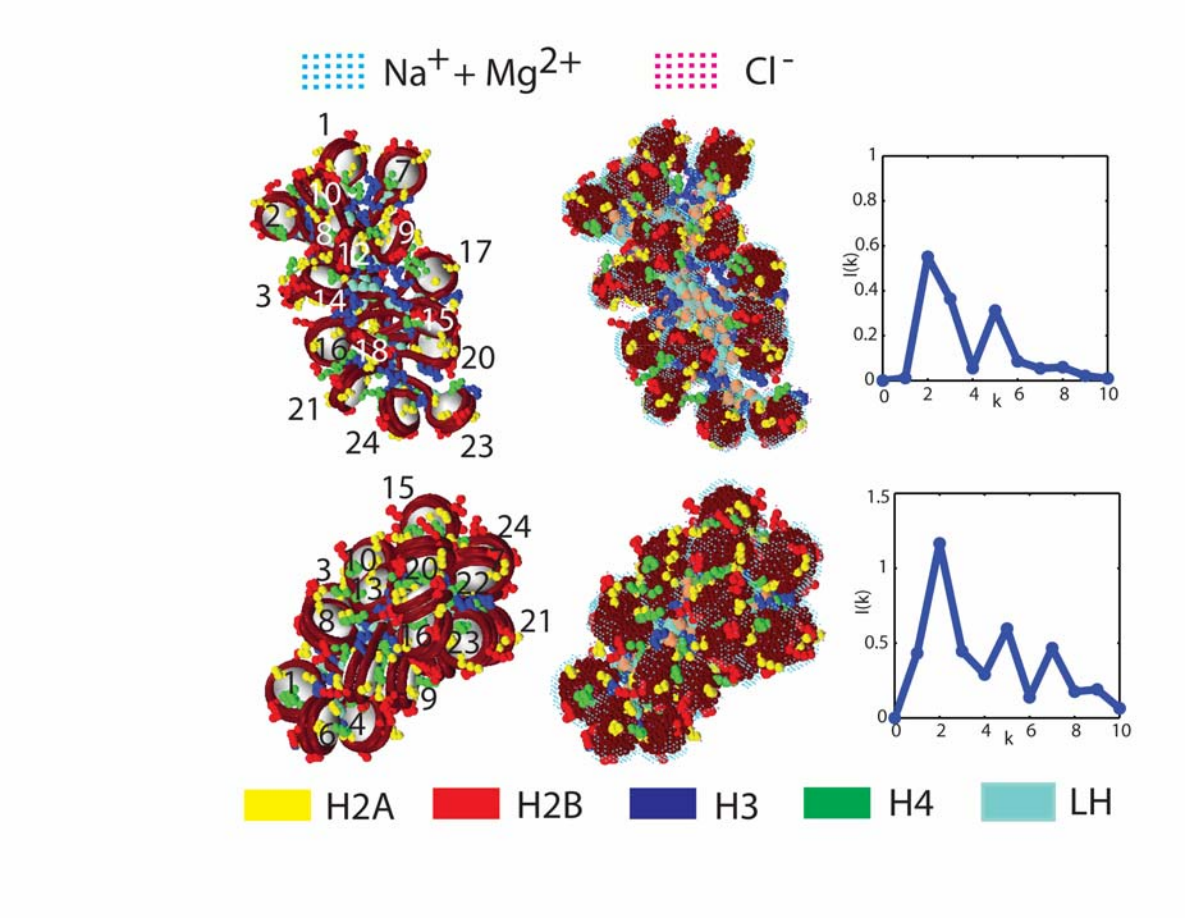

Fig. S7 (Fig. 5 in paper)
Distributions of counterions around an open (upper row) and compact (lower row) 24-core chromatin conformations from MC simulations at 10 million steps sampled at 0.15M NaCl salt and mixed 0.15M NaCl and $MgCl_2$ salts, respectively. Left column: chromatin folds with labeled cores (1 to 24) without their ionic clouds; middle column: ionic distributions of conformations evaluated at 0.15M NaCl salt (top) and mixture of 0.15M NaCl and 0.01M $MgCl_2$ salts (bottom); right column: internucleosome interaction intensity I(k) plots. Cation (cyan dots) and anion (magenta dots) density regions greater than 1.5 times the bulk ionic concentration are displayed.

Table S1. Fraction of shielding charge $\overline{Q}_\alpha$ in chromatin components at various NaCl concentrations.

Concentration(M)	Nucleosome	Linker DNA	Histone tails	Linker histone
0.05	0.7982	0.0977	0.0714	0.0328
0.10	0.8206	0.1007	0.0455	0.0331
0.15	0.8352	0.1030	0.0286	0.0332
0.20	0.8454	0.1046	0.0169	0.0332
0.25	0.8527	0.1057	0.0085	0.0331
0.30	0.8583	0.1066	0.0022	0.0329

Table S2. Fraction of shielding charge $\overline{Q}_\alpha$ in chromatin components at various $MgCl_2$ concentrations.

Concentration(M)	Nucleosome	Linker DNA	Histone tails	Linker histone
0.05	0.8549	0.1089	0.0024	0.0337
0.10	0.8866	0.1146	–0.0354	0.0341
0.15	0.9003	0.1172	–0.0514	0.0339
0.20	0.9001	0.1175	–0.0509	0.0333
0.25	0.8933	0.1169	–0.0429	0.0327
0.30	0.8839	0.1153	–0.0315	0.0323

Table S3. Symmetric charge fluctuation matrix $\hat{Q}_{\alpha\beta}$ at 0.15M NaCl.

Chrom. comp.	Nucleosome	Linker DNA	Histone tails	Linker histone
Nucleosome (C)	0.2607	–0.0205	2.0073	0.0282
Linker DNA (D)		0.5818	–2.0780	0.3854
Histone tails (T)			40.5065	–0.8128
Linker histone (LH)				2.2352

Table S4. Bare charges of chromatin beads

Nucleosome's 300 bead charges (e) at zero ionic concentration

1	-0.2573
2	-0.7857
3	0.9927
4	-0.5609
5	-0.0363
6	-0.1000
7	1.6115
8	0.4526
9	1.4014
10	-0.8982
11	-0.8580
12	-0.7987
13	-0.3352
14	0.1018
15	1.2879
16	-0.0615
17	-0.6395
18	0.0820
19	-0.2399
20	-0.0023
21	0.7650
22	-0.0704
23	-0.8362
24	3.9972
25	0.2063
26	-0.6694
27	0.0749
28	0.0680
29	-0.4913
30	-0.1514
31	-0.5744
32	-0.4007
33	-0.8165
34	0.4489
35	-0.0230
36	-1.1525
37	0.0042
38	-0.8708
39	-0.3110
40	-0.3657
41	-0.3551
42	-0.5758
43	1.8143
44	-1.8166
45	-0.8653
46	0.7111
47	-0.2469
48	-0.0795
49	0.1532
50	0.3635
51	-0.0881
52	-0.5116

53	-0.1627
54	0.3396
55	0.2819
56	-0.2247
57	-1.2989
58	-1.0826
59	-0.4671
60	0.2218
61	1.2438
62	0.7376
63	0.0991
64	4.3976
65	-0.1920
66	-0.0848
67	0.2468
68	-0.5543
69	-0.5477
70	0.0162
71	0.7009
72	0.7288
73	-1.1401
74	-2.0428
75	-1.2549
76	0.0436
77	-1.1544
78	1.6784
79	0.3725
80	1.2679
81	-1.2644
82	-0.3299
83	-0.4903
84	-0.2409
85	-0.2413
86	-1.2289
87	0.1514
88	-1.1688
89	-1.5325
90	-1.5968
91	0.1773
92	0.4332
93	0.5845
94	-0.5310
95	0.5582
96	-0.0846
97	-2.2017
98	0.5359
99	-2.1558
100	-0.4439
101	-1.4202
102	-0.7312
103	-1.6454
104	-1.9264
105	-1.5437
106	-2.0835
107	0.4351
108	-0.2671
109	-1.4388

110	-0.7231
111	-2.4967
112	-2.1358
113	-1.7751
114	-0.7164
115	-1.5535
116	-1.8252
117	-1.1081
118	-2.0479
119	-3.5226
120	-4.0623
121	-1.2804
122	-0.2230
123	0.7152
124	-1.7687
125	-2.5371
126	-2.0734
127	-1.0790
128	-1.6790
129	-1.2499
130	-2.1914
131	-1.9533
132	-2.3367
133	-3.1234
134	-0.8354
135	-1.7506
136	0.0872
137	-2.0795
138	-1.4917
139	-1.4023
140	-2.2887
141	-2.0087
142	-1.4439
143	-1.9725
144	-2.5598
145	-1.1479
146	-0.2990
147	-2.1941
148	-2.6902
149	-2.3357
150	-2.1547
151	-2.2448
152	-1.7144
153	-1.4176
154	-0.7157
155	0.0204
156	-0.8822
157	-0.7233
158	-0.0714
159	-2.5130
160	-2.2997
161	-2.1045
162	-1.6986
163	-0.8846
164	-1.1818
165	-2.0840
166	-2.1598

167	0.0966
168	-0.8024
169	-0.3304
170	-0.6833
171	-3.0340
172	-1.7380
173	-2.9723
174	-1.5667
175	-1.0608
176	-0.4223
177	-1.0778
178	-2.8261
179	-1.6427
180	-1.6564
181	-0.3562
182	0.0562
183	-1.9950
184	-1.1798
185	-1.8450
186	-1.4435
187	-0.9523
188	-1.5210
189	-0.6142
190	-0.6686
191	-1.1086
192	-2.0141
193	-1.7017
194	-0.0249
195	-0.4826
196	-1.1001
197	-0.7780
198	-1.0119
199	-0.8327
200	-1.3304
201	-0.2474
202	-0.3338
203	-0.9281
204	-0.8937
205	-0.4485
206	0.0470
207	-1.5109
208	-1.0846
209	0.0085
210	0.8938
211	1.1437
212	-0.4333
213	0.0124
214	-0.2488
215	-0.8805
216	-0.4593
217	-1.2188
218	-0.0786
219	-0.1673
220	-0.8034
221	-0.5234
222	-1.0287
223	0.3350

224	0.1924
225	-0.2695
226	1.6764
227	0.3883
228	-0.2122
229	1.0167
230	-0.3397
231	0.5145
232	-0.7233
233	0.1189
234	-1.2838
235	-0.9245
236	-0.4656
237	-0.2197
238	-0.3508
239	-0.7742
240	-0.5173
241	-0.0824
242	-0.4865
243	0.5636
244	0.8717
245	-0.0185
246	0.0251
247	-0.1476
248	-0.2454
249	-0.2323
250	-0.3585
251	0.4170
252	-0.2578
253	0.2481
254	-0.8987
255	0.4229
256	-0.2961
257	0.3936
258	0.1161
259	0.5445
260	0.4759
261	0.5077
262	-0.1309
263	-0.8024
264	-1.1980
265	0.7180
266	0.5656
267	-0.5209
268	-0.0881
269	0.0993
270	0.0618
271	-0.2747
272	-0.9755
273	0.8880
274	-0.9375
275	0.0450
276	0.9118
277	-0.0671
278	0.7935
279	-0.0441
280	-0.6816

```
281          -0.4430
282          -0.3438
283           0.8506
284          -0.0664
285           0.3457
286           0.5612
287          -0.7160
288          -0.3941
289           1.4738
290           1.1745
291          -0.3394
292          -0.1433
293           0.7102
294           0.1551
295           0.7765
296          -0.9863
297          -0.4685
298          -1.0449
299           0.6191
300           1.8360
```

Charge (e)/DNA bead -17.6471

Charges on flexible histone tails

Histone protein	Chain	Charges on bead model (e)
H3A	A, E	+3,+2,+1,+2,+1,+2,0,+3
H4B	B, F	+3,+1,+1,+4,0
H2A	C, G	+3,+1,+3,+2
H2A	C, G	+1,0,+2
H2B	D, H	+2,+2,+2,+2,+2

Charges on linker histone

Linker histone domain	Charge (e)
globular domain bead	8.3164
C-terminal domain bead 1	16.8123
C-terminal domain bead 2	16.8123

Table S5. Radii of chromatin beads.

Chromatin component	Bead radius (Å)
Nucleosome core	6
Linker DNA	30
Histone tails	9
Linker histone (globular and C-terminal domains)	17 and 18